Mechanism of Nucleotide-Dependent Allosteric Regulation in *Escherichia coli* Aspartate Transcarbamoylase

Robert C. Miller[1,*], Michael G. Patterson[1,*], Neti Bhatt[2], Xiaokun Pei[1], and Nozomi Ando[1,2†]

[1]Department of Chemistry and Chemical Biology and [2]Department of Physics,

Cornell University, Ithaca, NY 14853, USA.

[*]These authors contributed equally.

[†] Correspondence should be addressed to nozomi.ando@cornell.edu.

Abstract

Discovered nearly 70 years ago, the allosteric regulation of *Escherichia coli* aspartate transcarbamoylase (ATCase) is discussed in every biochemistry textbook. ATCase catalyzes the first step in pyrimidine biosynthesis. Despite extensive research, the mechanism by which this enzyme is regulated by pyrimidine and purine nucleotides has remained elusive. Here, we present a detailed analysis of *E. coli* ATCase using a combination of biochemical assays, small-angle X-ray scattering (SAXS), cryo-electron microscopy (cryo-EM), and X-ray crystallography, revealing the mechanism of allosteric communication between nucleotide-binding sites and active sites. We show how the pyrimidine pair, CTP and UTP, synergistically inhibit the enzyme by inducing a quaternary structure that enforces active-site cooperativity. Additionally, we provide the first evidence of how the purine pair, ATP and GTP, drive the enzyme into its most active state by promoting an expanded conformation that allows independent function of the active sites. Our findings resolve longstanding questions in the literature and uncover a novel mechanism by which *E. coli* ATCase regulates the balance of pyrimidines and purines.

Introduction

Escherichia coli ATCase has served as an enduring example of allostery for nearly 70 years.[1–3] ATCase sequentially binds two substrates, carbamoyl phosphate (CP) and L-aspartate (Asp), to catalyze the committed step of the pyrimidine biosynthesis pathway, which results in the production of uridine 5′-triphosphate (UTP) and cytidine 5′-triphosphate (CTP) (Figure 1A). Seminal biochemical studies revealed that the pathway end-product CTP inhibits ATCase by inducing cooperative behavior with respect to the second substrate, Asp, while the purine nucleotide adenosine 5′-triphosphate (ATP) stimulates activity.[4] Later studies showed that UTP acts synergistically with CTP to enhance inhibition,[5] while the role of guanosine 5′-triphosphate (GTP) has been less clear.[4,6–9] Remarkably, despite decades of research, the precise mechanism by which nucleotides regulate this well-known enzyme had remained elusive.

Numerous models have been proposed to explain the regulation of ATCase activity,[8–17] which famously exhibits a sigmoidal dependence on the second substrate, Asp. Of these, the most influential has been that of Monod, Wyman, and Changeux (MWC), whose work was contemporaneous with initial biochemical characterizations of ATCase.[10–12] In the MWC framework, the sigmoidal dependence is explained by the interconversion between two preexisting conformations, where substrate binding shifts the equilibrium in a cooperative manner from a so-called tense (T) state, which has low substrate affinity, to a relaxed (R) state, which has high substrate affinity. According to this model, allosteric inhibitors shift the equilibrium towards the T-state, while activators shift the equilibrium towards the R-state.

Consistent with such a model, crystallographic studies spearheaded by Lipscomb, Kantrowitz, and coworkers over the course of 45 years have revealed two major conformations (Figure 1B-D), regardless of whether nucleotides are bound.[9,14,18–25] *E. coli* ATCase has a distinctive dodecameric architecture with two trimers of the catalytic subunit arranged with their active sites facing each other, bridged by three dimers of the regulatory subunit with nucleotide-binding sites facing outwards (Figure 1B-D). Substrates bind the catalytic subunit via the reorganization of two active-site loops, known as the 80s loop (residues 74-88) and 240s loop (residues 229-247) (Figure 1B), to produce a dramatic opening of the enzyme complex via a screw-like mechanism. The closed and open conformations depicted by crystallography have been widely accepted in the literature to represent the T- and R-states (Figure 1D). However, although significant efforts have been made, existing crystal structures of nucleotide-bound ATCase have fallen short of explaining how the identity of nucleotides at the regulatory subunits is communicated to the catalytic subunits.

Efforts to understand allostery in ATCase have been complicated by several factors, including the lack of standardized conditions for direct comparisons of structural and biochemical data. Notably, the metal dependence of ATCase had not been considered consistently. The final crystal structures from the Kantrowitz group, reported about a decade ago, confirmed that there is not one but two nucleotide-binding sites per regulatory subunit in the presence of Mg^{2+}.[6,9,24,25] Additionally, Vachette and colleagues demonstrated that crystal structures of the R-state could not be reproduced by small-angle X-ray scattering (SAXS), highlighting the need for more solution-based studies.[29]

Based on these observations, we conducted a comprehensive biochemical and structural study of *E. coli* ATCase under uniform, physiologically relevant conditions at pH 7.5 and with 15 mM Mg^{2+}. Using activity assays, SAXS, cryo-EM, and crystallography, we systematically addressed outstanding questions in the literature. We find that although ATCase generally adheres to a two-state model in response to substrate

binding, the identity of the nucleotides bound at the regulatory dimers results in distinct R-state ensembles with varying degrees of expansion. Our findings imply that nature has evolved an elegant allosteric mechanism for ATCase, where the pyrimidine pair, CTP and UTP, inhibits the enzyme by imposing highly cooperative behavior between the two catalytic trimers, while the purine pair, ATP and GTP, is uniquely able to relieve this inhibition by decoupling the catalytic trimers.

Discrepancy Between Crystallography and SAXS on the Nature of the R-state

We first examined the structural transition induced by the potent bisubstrate analog *N*-(phosphonoacetyl)-L-aspartate (PALA)[28] using SAXS and showed that this transition can also be driven by CP and the Asp analog, succinate (Supp. Fig.1, Supp. Table 1). The scattering of *E. coli* ATCase displays a prominent secondary peak that reflects the extent of quaternary expansion (Figure 1E, arrow). When visualized in a Kratky plot (Iq^2 vs q), we observe a 1.6-fold increase in peak height and a shift to lower q from ~0.122 to ~0.112 Å^{-1}, indicating that the enzyme expands to a more open structure. Singular value decomposition (SVD) revealed that both datasets can be described as a two-state T-R transition (Supp. Fig. 1). The scattering of ligand-free ATCase, which represents the solution T-state, is described well by the crystallographic T-state (Figure 1E, blue). However, as noted by Vachette and co-workers,[9] the crystallographic R-state is not expanded enough to describe the observed position of the secondary peak in the solution R-state (Figure 1E, red).

SAXS Reveals the Effect of Nucleotides on the R-state in Solution

A key assumption of the MWC model is that nucleotides affect enzyme activity by shifting the equilibrium between two conformational states with differing affinities for the substrate. To test this assumption, we saturated ATCase with CP and succinate to obtain the R-state and then performed SAXS experiments at varying nucleotide concentrations (Supp. Tables 2-3).

Addition of CTP to the R-state resulted in a two-state transition, with a small shift in the secondary peak towards higher q (Supp. Fig. 2A). However, the peak position plateaued around 2 mM CTP well before reaching the T-state value of 0.122 Å^{-1}, suggesting that a slightly contracted form of the R-state had been induced. Titration with equimolar CTP and UTP produced a similar but slightly more pronounced two-state transition, plateauing at ~0.118 Å^{-1} above 1 mM (Supp. Fig. 2A). Purines induced two-state transitions in the opposite directions, suggesting an expansion of the R-state (Supp. Fig. 2B). The canonical activator ATP led to a slight increase in the secondary peak height saturating above 2 mM, while titration of GTP at a fixed ATP concentration of 5 mM led to further expansion, with the peak increasing in height and shifting to lower q (~0.104 Å^{-1}). Notably, this transition saturated at a low concentration of 250 μM GTP, suggesting significance for the ATP/GTP pairing.

To examine the subtle effects of nucleotides with greater confidence, size-exclusion chromatography-coupled SAXS (SEC-SAXS) was performed under conditions identified above that saturate the unliganded T-state, nucleotide-free R-state, and the various nucleotide-bound R-states (Supp. Tables 4-6). In all cases, model-free deconvolution led to a clean signal separation of the ATCase complex (Figure 2A) from a minor higher-order species (Supp. Fig. 3-5). The resulting high-quality scattering profiles recapitulate the observations from titration experiments. In addition to the expected shift in the secondary peak from 0.122 Å^{-1}

for the unliganded T-state to 0.112 $Å^{-1}$ for the nucleotide-free R-state, a gradient of peak positions is observed for the nucleotide-bound R-states, with pyrimidines and purines shifting the peak in opposite directions (Figures 2A, Supp. Fig. 6), corresponding to compaction and expansion, respectively. Altogether, our SAXS results confirm that although substrate binding induces a concerted transition as predicted by the MWC model, nucleotides alter the quaternary structure of the R-state with the pyrimidine and purine pairs, CTP/UTP and ATP/GTP, having the most pronounced effects.

Cryo-EM Captures Nucleotide Effects on the T-R Equilibrium and Quaternary Structure

To visualize the effects of nucleotides on quaternary structure, we examined *E. coli* ATCase by cryo-EM under the same set of conditions used for SEC-SAXS (Supp. Fig. 7-14, Supp. Tables 7-8). 3D classification of intact ATCase particles yielded two types of 3D classes across all datasets: those that are T-state-like (closed) and those that are R-state-like (open). As expected, only a T-state-like class was observed for the unliganded ATCase, and the consensus model agreed well with the scattering profile obtained by SEC-SAXS (Figure 2A). For all other datasets, which were obtained with saturating concentrations of CP and succinate, R-state-like classes were observed. Of these datasets, those obtained with pyrimidines (CTP alone or CTP/UTP together) also contained a small T-state-like class, corresponding to 16-25% of the particles (Supp. Fig. 8-9, 15).

From these datasets, three T-state and five R-state consensus maps were obtained with overall resolutions of 2.6-3.9 Å estimated by Fourier shell correlation. The enzyme interior, including the active sites, generally aligned to higher resolution (~2.5-3.0 Å) than the allosteric sites (~2.8-4.5 Å) located on the outer periphery (Supp. Fig. 7-12). In all maps obtained with CP and succinate, density for CP was clearly visible, while density for succinate was more variable, reflecting its weak binding compared to the actual substrate, Asp. Regardless, a key distinguishing feature between T-state and R-state maps was the absence or presence of any succinate density (Supp. Fig. 13). Consistent with this observation, density for the R234 on the 240s loop, which is responsible for binding succinate, is observed engaged in all active sites in R-state maps, while they are disengaged in T-state maps (Supp. Fig. 13).

Consensus models of the T-state were highly similar to each other (Cα root-mean-square deviations of 0.8-1.1 Å). However, a gradient of R-state structures is observed, with pyrimidine and purines respectively inducing a compaction and expansion (Figure 2B). These changes are readily visualized by the 240s loops, which come nearly into contact in the presence of pyrimidines but are far apart in the presence of purines (Figure 2B, bottom row). Importantly, these R-state models agree well with the scattering profiles obtained by SEC-SAXS under matching conditions (Figure 2A). The only scattering profile that is slightly better described by a T- and R-state mixture is that obtained with CTP/UTP (Supp. Fig. 15A). Here, the best fit is obtained with a 20:80 mixture of the T- and R-state models obtained from this condition, similar to the 25:75 distribution of particles estimated by 3D classification. For the scattering profile obtained with CTP alone, the best fit was obtained with the corresponding R-state model on its own (Supp. Fig. 15B).

To assess structural heterogeneity within each state, particles used for consensus refinement were subjected to symmetry expansion and 3D variability analysis (3DVA) (Supp. Fig. 7-12). For each state, the resulting 3DVA trajectory could be described by a single mode of continuous breathing-like motion, which was discretized into 20 unique sub-volumes. Refined models from corresponding consensus maps were then

rigid-body fit into the sub-volumes to convert the 3DVA latent variable into a physiologically meaningful coordinate: the center-of-mass distance between the catalytic trimers. The resulting histograms reveal a small spread within each conformational ensemble (Figure 2C). Compared to crystal structures of the R-state which consistently display trimer distances of 55.9 ± 0.3 Å (Methods), the R-state ensembles from cryo-EM are clearly more expanded, with mean trimer distances ranging from 57.4 to 62.4 Å.

These observations support the idea that the R-state is flexible enough to collapse in a crystal lattice, and that this flexibility is important for nucleotide-dependent regulation. Notably, although we do observe a small population of T-state by both cryo-EM and SAXS with CTP/UTP, the effect of pyrimidines is not simply to shift the T-R equilibrium – they clearly cause a compaction of the R-state. Moreover, the R-state ensemble obtained ATP/GTP is significantly more expanded than all other states, further highlighting the significance of this pairing of purines.

Correlation with Enzyme Activity

Because enzyme kinetics have not been reported at pH 7.5 in the presence of Mg^{2+}, we performed activity assays at the same nucleotide concentrations used for SEC-SAXS and cryo-EM (Figure 2D). The CP concentration was fixed at 4.8 mM, and the initial rate was measured at variable Asp concentrations. It was previously shown at pH 7.0 and 8.3 that CTP on its own does not have a strong inhibitory effect in the presence of Mg^{2+} and that this metal ion plays an important role in coordinating the binding of two nucleotides in each regulatory subunit.[30] Consistent with this work, we find that it is the combination of CTP and UTP that is most inhibitory, while the combination of ATP and GTP is most activating at physiological Asp concentrations of ~4.2 mM (Figure 2D, inset).[30]

The pyrimidine pair produces a highly sigmoidal saturation curve, while that produced with the purine pair appears hyperbolic at low Asp concentrations. At high Asp concentrations, it is known that ATCase exhibits behavior that is suggestive of substrate inhibition (i.e., a downturn in activity), however this effect is not well understood and is difficult to model with low uncertainties.[31] We thus performed fits to the Hill equation in the transition regions where this model is suitable (Supp. Fig. 16, Supp. Table 9). This analysis reveals that the Hill coefficient n_H and the Asp concentration needed to reach half-maximal activity $K_{1/2}$ are inversely correlated with the openness of the R-state observed by cryo-EM and SAXS.

Two important conclusions can be drawn: (1) CTP and UTP together inhibit ATCase by inducing a compaction of the R-state to produce highly cooperative behavior (n_H ~2.9), rendering the enzyme virtually inactive near physiological [Asp] ($K_{1/2}$ ~37 mM), whereas (2) ATP and GTP together produce the most expanded R-state, where cooperative behavior is largely lost (n_H ~1.2) and the enzyme is highly active at physiological [Asp] ($K_{1/2}$ ~ 2.9 mM). Since the cellular concentrations of the four nucleotides[23,31,32] exceed the levels needed to saturate the structural effects induced by the CTP/UTP pair or the ATP/GTP pair (Supp. Table 10), it is likely that these paired binding modes are more physiologically relevant than ATCase bound to only one type of nucleotide or none at all.

Crystallography Resolves Unusual Binding of ATP and GTP

To obtain high-resolution insight into the nucleotide-binding sites, crystallography was performed in parallel to cryo-EM (Supp. Table 11). Previous crystallographic work by Kantrowitz and co-workers had revealed how the pyrimidine pair, CTP/UTP, binds the regulatory subunit in the presence of Mg^{2+}.[31] With CTP in the first binding site, a Mg^{2+} ion enables the preferential binding of UTP in a second site, which in turn recruits the flexible N-terminus of the regulatory subunit (Figure 3A). They also reported a PALA-bound structure with two ATP molecules coordinated by Mg^{2+}. However, the weak density suggested that ATP may not be the optimal ligand in the second site.

Because all previous crystal structures of nucleotide-bound *E. coli* ATCase were obtained at acidic conditions (pH 5.7-5.9), we screened for new co-crystallization conditions that would clarify how purines interact with the enzyme at neutral pH. We first reproduced results from the Kantrowitz group by obtaining a 3.0-Å resolution structure of ATCase bound with ATP, CP, and succinate (Figures 3D, Supp. Fig. 17-18). As with the previous structure, density for ATP in the second site is weaker than that in the first site, and the N-termini of the regulatory subunits reach across the dimer interface without forming an ordered structure.

We then identified a co-crystallization condition at neutral pH that produced a new P321 crystal form of ATCase bound with ATP, GTP, and PALA (Supp. Fig. 19). A 2.1-Å resolution structure was obtained at room temperature at a pH between 7.0-7.5 with strong electron density in the regulatory subunit supporting the assignment of ATP in the first site and GTP in the second site, coordinating a shared Mg^{2+} ion (Figures 3B-C, Supp. Fig. 20). Unlike the structures with disordered ATP in the second site (Figure 3D), here, we observe ordered GTP molecules forming a non-canonical base pair across the dimer interface (Figure 3C). For such pairing, one GTP must be deprotonated at the N1 position at any given time. Although the pKa at this position is 9.2 in free GTP, electronic structure calculations suggest that it can be shifted towards neutrality by a positive charge on the Hoogsteen face of the nucleobase, which stabilizes its deprotonated form, where negative charge is resonance-distributed between N1 and O6.[32] In ATCase, a conserved K60 provides this positive charge (Supp. Fig. 21). Such a mechanism would explain why a GTP-bound structure was not obtained in the previously used, acidic crystallization conditions as well as why our crystals dissolved at lower pH.

Comparison of structures with CTP/UTP and ATP/GTP reveals how nucleotide identity affects the flexible N-terminus of the regulatory subunit. As has been noted before, the first nucleotide-binding site is specific for the amino group and the adjacent nitrogen of CTP or ATP and hence cannot make favorable interactions with UTP or GTP. Notably, when CTP or ATP binds this site, the amino group forms hydrogen bonds with the backbone carbonyls of I12 and Y89, while the adjacent nitrogen makes an additional bond with the backbone amide of I12 or A11. These interactions serve to couple the N-terminus (residues 1-14) with the "outer loop" (residues 88-89, stars in Figure 3A-B) that connects the two outermost β-strands of the regulatory subunit. K60 links the two allosteric sites, favoring interactions with the carbonyl oxygen of a UTP or GTP than the amino group of a CTP or ATP in the second site. Thus, with CTP in the first site, the N-terminus wraps around UTP in the second site to form additional base-specific interactions, bringing the two N-termini together at the dimer interface to form a barrier between each CTP/UTP pair (Figure 3A). Conversely, with ATP in the first site, K60 selects for GTP in the second site and stabilizes non-canonical base-pairing across the dimer interface, resulting in a 4-nucleotide unit (Figure 3B-C). Here, the N-terminus from each regulatory subunit reaches across the dimer interface to form a domain-swapped antiparallel β-sheet above the plane of the nucleotides, making hydrophobic interactions with the GTP bases. Altogether,

these observations explain the previously observed importance of the N-termini in allosteric regulation[23,33,34] and highlights the specific interactions made by the ATCase regulatory subunit with the pyrimidine pair CTP/UTP and the purine pair ATP/GTP.

Allosteric Communication Revealed

To understand how nucleotide binding at the regulatory subunits propagates to the active sites, we combined the strengths of cryo-EM and crystallography. Cryo-EM model refinement was performed with starting models built from high-resolution crystal structures, and non-crystallographic symmetry (NCS) restraints were applied to systematically characterize regions of asymmetry across the ATCase complex (Methods, Supp. Fig. 22).

The refined cryo-EM models reveal a clear nucleotide-dependent path for allosteric communication (Figure 3E-G). The regulatory subunits form an extended β-sheet across the dimer interface, where the outer face makes polar interactions with nucleotides, while the inner face, which consists almost entirely of isoleucines, makes hydrophobic interactions with two pairs of helices, H1 and H2 (Figure 3E-F). The H2-helix makes direct contact with the Zn domain, which is responsible for binding a catalytic subunit. Remarkably, nucleotide binding controls the bending angle of the regulatory dimers, which in turn controls the center-of-mass distance between the catalytic trimers (Figure 3G).

Binding of ATP/GTP produces the most bent β-sheet (9.3° from planar), facilitated by the N-termini reaching over the GTPs in the second site and pulling on the outer loops through interactions mediated by ATP in the first site (Figure 3B). This action in turn pulls on the linkers between the nucleotide-binding and Zn domains (Figure 3F), such that a slight overall bending of the regulatory dimer becomes amplified into a large separation between the Zn domains and hence the catalytic trimers. Interestingly, the linker residues P97 and P100 form a groove around the outer H2-helix, and bending of the regulatory dimer is accompanied by its repacking. In the T-state, the H2-helices within a regulatory dimer are angled in opposite directions (Supp. Fig. 22D), but in the ATP/GTP-bound R-state, these helices straighten into a parallel configuration (Figure 3F, Supp. Fig. 22A).

In contrast, binding of CTP/UTP leads to a nearly planar β-sheet (3.1° from planar), facilitated by the N-termini acting as a spacer between the nucleotide pairs at the dimer interface (Figure 3A). Correspondingly, the separation between the Zn domains is smaller than that in the ATP/GTP-bound R-state while also being larger than that in the T-state. This intermediate level of expansion leads to asymmetry: within each regulatory dimer, one H2—helix is angled like in the T-state (H2 in Figures 3E, Supp. Fig. 22B) while the other is straightened like in the ATP/GTP-bound R-state (H2′ in Figure 3E, Supp. Fig. 22B). This unusual asymmetry is in fact also observed in crystal structures of the R-state (Supp. Fig. 22C) and was thought to explain the existence of high- and low-affinity sites for CTP or ATP before it was known that there are two distinct sites per regulatory subunit. Our cryo-EM models reveal that this asymmetry is only a feature of collapsed forms of the R-state and that crystal structures of the R-state most closely resemble the CTP/UTP-bound R-state in solution.

Altogether, our results are consistent with the purine pair ATP/GTP producing the most expanded R-state, where the catalytic trimers are fully separated, and the pyrimidine pair CTP/UTP producing a compressed R-state structure, where the catalytic trimers are held closer together.

Cooperativity of the 240s Loop

Our findings so far indicate that nucleotide-dependent regulation of ATCase involves bending of the regulatory dimers, which controls the separation between the catalytic trimers and the binding cooperativity of the second substrate. To further explore the link between nucleotide binding and cooperativity, we examined the individual roles of substrates and nucleotides using SAXS. Surprisingly, addition of ATP/GTP at the same concentrations used in our other experiments induced a substantial shift of the secondary scattering peak to lower q even in the absence of substrates (Figure 4A-B, green). When CP was added along with ATP/GTP, the peak shifted all the way to the position observed for the ATP/GTP-bound R-state obtained with both substrates (Figure 4A-B, orange/red). No other nucleotide combination induced a significant structural change in the absence of substrates or with CP alone (Figure 4A-B), suggesting that ATCase has uniquely evolved to interact with ATP/GTP.

To gain molecular insight into the unexpected behavior observed by SAXS, we performed cryo-EM and obtained a ~3.2-Å resolution reconstruction of ATCase in a fully open conformation bound only to the first substrate CP and the nucleotide pair ATP/GTP (Supp. Fig. 23, Supp. Table 7). The refined model exhibits a trimer distance of 62.5 Å and is consistent with the scattering profile obtained under identical solution conditions (Supp. Fig. 24). A defining feature of this novel state is the conformations of the active-site loops: the 80s loops are bound to CP, but the 240s loops are disengaged, extending into the central opening of the enzyme (Figure 4D). In the closed T-state, the 80s loops can bind CP (Supp. Fig. 13), but the 240s loops are restricted from moving. As a result, it had long been believed that binding of both substrates, which requires both the 80s and 240s loops to engage (Supp. Fig. 13), drives the opening of the enzyme to the R-state conformation.

Here, we show that when ATCase is bound to ATP/GTP, binding of CP is sufficient to fully open the enzyme into a conformation that would allow unrestricted movement of the 240s loop. As this conformation represents a state with high affinity for Asp, it is part of the R-state ensemble, and we can call it a “pre-Asp R-state”. When ATP/GTP are bound, the pre-Asp R-state is expanded enough that the 240s loops can remain extended without clashing with those of the opposing catalytic trimer. However, if we dock the catalytic subunits from the pre-Asp R-state into the cryo-EM structure of the CTP/UTP-bound R-state, a significant clash is observed between the catalytic trimers (Supp. Fig. 25). Performing this analysis with our other cryo-EM models shows that ATP/GTP is the only nucleotide combination that produces a sufficiently large separation of the catalytic trimers to comfortably allow all active sites to bind Asp independently of each other. Conversely, the movement of the 240s loops is more restricted with the other nucleotides, and thus the active sites cannot act as independently. These observations explain why the most compressed state, which is produced by CTP/UTP, exhibits the greatest cooperativity, and why cooperativity is lost in the most expanded state produced by ATP/GTP.

Discussion

Feedback regulation of ATCase was first observed in *E. coli* in 1956,[34] just a year before the dawn of structural biology.[35] Seminal biochemical studies then established that inhibition of ATCase by CTP presents as a sigmoidal dependence on the second substrate, Asp.[4] In the immediate years that followed, pioneering crystallographic studies on hemoglobin[27] and the development of the MWC model of allostery[35] provided a framework for understanding the sigmoidal behavior of ATCase in terms of two conformational states. In a remarkable feat that took two decades, crystallographic studies ultimately succeeded in revealing two major conformations: a closed state that is favored in the absence of substrates[28] and an open state that is favored when substrate analogs are bound.[36] Early SAXS studies further showed that substrate binding leads to a concerted transition between two such states.[37] Thus, overall, the MWC model was able to explain how sigmoidal substrate binding can arise from a T-state and R-state. Despite these successes, however, the original question of how nucleotides regulate ATCase remained unanswered.

In this study, we leveraged advances in structural biology to revisit the mechanism of allostery in *E. coli* ATCase. By applying model-free data decomposition methods[37,38] to SAXS data, we demonstrated that nucleotides do not simply shift the equilibrium between the T- and R-states, as assumed by the MWC model, and that in fact, both pyrimidines and purines alter the quaternary structure of the R-state. Findings from SAXS provided a roadmap for single-particle cryo-EM studies of ATCase, which allowed us to visualize how different nucleotide combinations result in a gradient of R-states, with pyrimidines causing a compaction and purines causing an expansion. These analyses revealed that the R-state exhibits functionally important flexibility and can therefore partially collapse in a crystal lattice, providing an explanation for a long-standing discrepancy between SAXS and crystallography[38,39] and why significant nucleotide-dependent changes had not been previously captured. However, where cryo-EM excels at capturing the flexibility of a protein, crystallography provides a means for limiting structural disorder. By pursuing crystallography in parallel and moving away from the acidic conditions used in past studies, we were able to obtain detailed insight into how GTP, a nucleotide that has often been overlooked in the ATCase literature, pairs with ATP.

By integrating our structural findings with biochemical data, we are able to propose a new mechanism for nucleotide-dependent regulation of *E. coli* ATCase (Figure 5). Although a protein, which is dynamic and flexible, cannot be directly compared to a mechanical device, an analogy can be made between the V-shaped regulatory dimer and a bicycle brake, where the Zn domains serve as the brake pads. When ATP and GTP are bound to the outer face of the regulatory dimer, the N-termini wrap above the plane of the nucleotides, pulling on outer edges to open up the spacing between the Zn domains. Conversely, when CTP and UTP are bound to the outer face, the N-termini wrap around the nucleotides in-plane, forcing the surface to flatten and causing the regulatory dimer to partially collapse and bring the Zn domains together. These motions, in turn, directly affect the reaction rate and cooperativity of the enzyme because the active-site 240s loop must move within the confined space of the enzyme cavity. Binding of the CTP/UTP pair is analogous to putting the brakes on the enzyme by compressing the space available for the 240s loops to move, whereas the ATP/GTP pair minimizes this effect (Figure 5). In the latter state, the enzyme functions more like a catalytic trimer on its own, and consistent with this, removing the regulatory subunit from *E. coli* ATCase results in an increase in activity and loss of cooperativity.[4] We note that although many bacterial ATCases have a regulatory subunit, there is also a class of ATCases that function as catalytic trimers.[40–42] Thus, it is interesting that the regulatory subunit evolved to allow ATCase to tune between unregulated and regulated states. Such a function is undoubtedly linked to the unusual structural features of

the regulatory dimer, such as the striking difference in amino acid composition above and below the extended β-sheet that enables ordered nucleotide binding on one side to cause repacking of the helices and Zn domains on the other side.

Finally, we address the likely physiological nucleotide states for *E. coli* ATCase. Given the estimated concentrations of nucleoside triphosphates (NTPs) in the cell, which are on the order of millimolar, we believe that a nucleotide-free state is rare. With physiological levels of Mg^{2+}, the regulatory subunits are selective for the binding of two NTPs, preferring the chemical features of CTP or ATP in the first site, which in turn selects for UTP or GTP in the second (Figure 5). For these nucleotide combinations, the flexible N-termini of the regulatory subunits adopt meaningful, ordered conformations. In agreement with work by others,[43] we have found that the regulatory subunit can bind two molecules of CTP or ATP (Supp. Fig. 14), but the conformation of the second-site nucleotide and the N-termini are not as well-ordered. Likewise, when Mg^{2+} is present, single-nucleotide conditions have much less pronounced effects on enzyme activity compared to the mixed-nucleotide pairs. Altogether, these findings strongly suggest that the CTP/UTP and ATP/GTP pairs are the most physiological nucleotide-binding modes. It is intriguing that nature evolved a complicated regulatory scheme that involves all four NTPs. Yet nucleotide metabolism is heavily regulated at many key steps, and other complex enzymes include ribonucleotide reductase,[40,41] which is allosterically regulated by multiple DNA precursors (dNTPs), and glutamine-phosphoribosyl pyrophosphate amidotransferase in the purine pathway,[42–44] which is regulated by multiple downstream purines. For ATCase, the preference for CTP in the first site and UTP in the second is especially significant as CTP is the final product and UTP is the penultimate product of the pathway it regulates. This ensures that the pathway is not inhibited until both products have accumulated. Likewise, the ATP and GTP pairing may have significance because the purine biosynthesis pathway is bifurcated, producing both products. Additionally, this pairing may endow ATCase with greater sensitivity to the abundance and balance of purines as ATP is also a substrate for CP synthesis.[45] Nonetheless, the symmetric use of pyrimidine and purine pairs makes regulation of ATCase particularly elegant. At last, 70 years of research has been synthesized into a unified story, closing this chapter on *E. coli* ATCase.

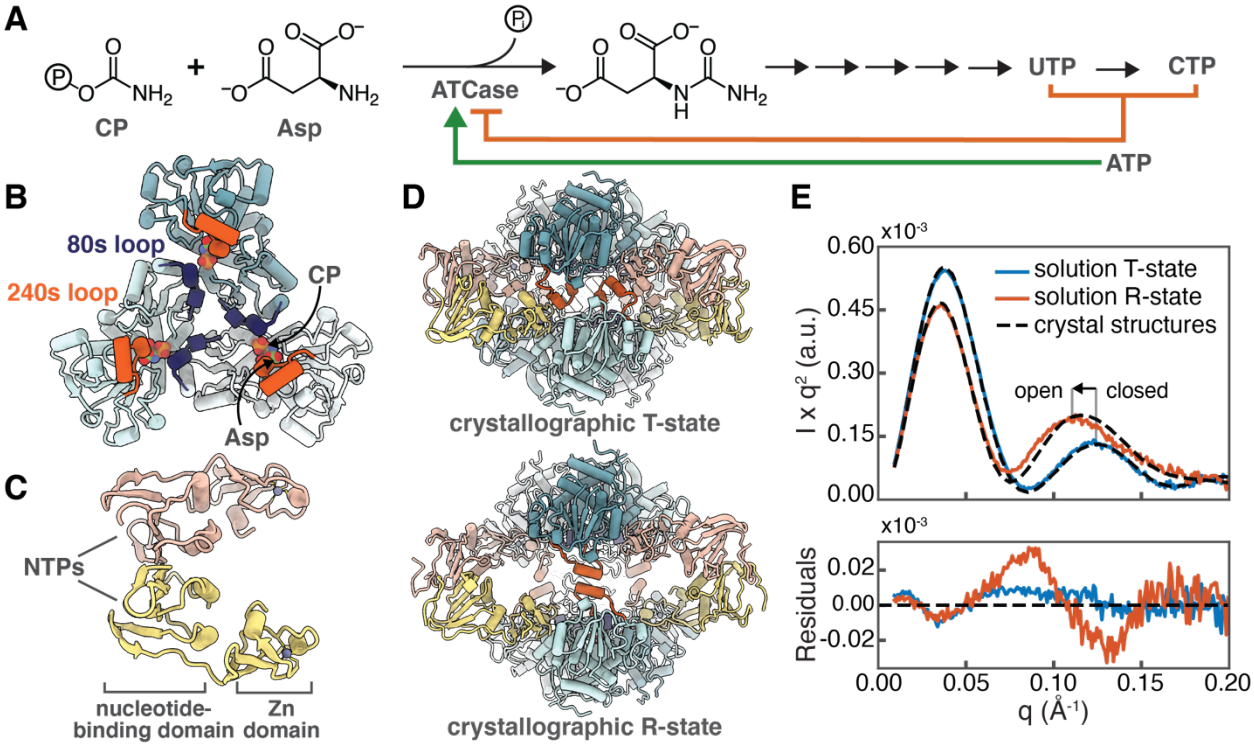

Figure 1. Regulation of *Escherichia coli* ATCase: knowns and unknowns. **(A)** Traditional regulatory scheme for ATCase. ATCase catalyzes the committed step of pyrimidine biosynthesis, the condensation of carbamoyl phosphate (CP) and L-aspartate (Asp). Early studies revealed that ATCase is inhibited by CTP, the pathway end-product, with its precursor UTP enhancing its effects, while ATP, a product of the purine biosynthesis pathway, stimulates activity.[4,5] The role of GTP has been debated.[4,6,9] **(B)** The catalytic subunit functions as a trimer, with each active site sequentially binding two substrates. CP binds first along with an 80s loop (*purple*) from a neighboring subunit, followed by Asp, which involves a large rearrangement of the 240s loop (*orange*) within the same subunit. **(C)** The regulatory subunit dimerizes at the nucleotide-binding domains, each binding a pair of nucleoside triphosphates (NTPs) in the presence of Mg^{2+}. Each Zn domain is responsible for binding a catalytic subunit. **(D)** *E. coli* ATCase forms a dodecamer comprising two catalytic trimers and three regulatory dimers. Crystal structures have historically depicted two major conformations, designated the tense (T) and relaxed (R) states, regardless of whether nucleotides are bound. **(E)** The crystal structure of the unliganded T-state (PDB: 6at1)[23] provides a good fit to the experimental SAXS profile of *E. coli* ATCase in the absence of ligands (*blue*). However, the PALA-bound R-state structure (PDB: 1d09)[6] does not fit the SAXS profile obtained with 50 μM PALA (*red*). The position of the second peak in the Kratky plot (Iq^2 vs. q) inversely correlates with the degree of expansion in the ATCase complex, indicating that in solution, the R-state is more expanded than depicted by crystallography. In panels B-D, the T-state structure is 6at1, while all others are 1d09.

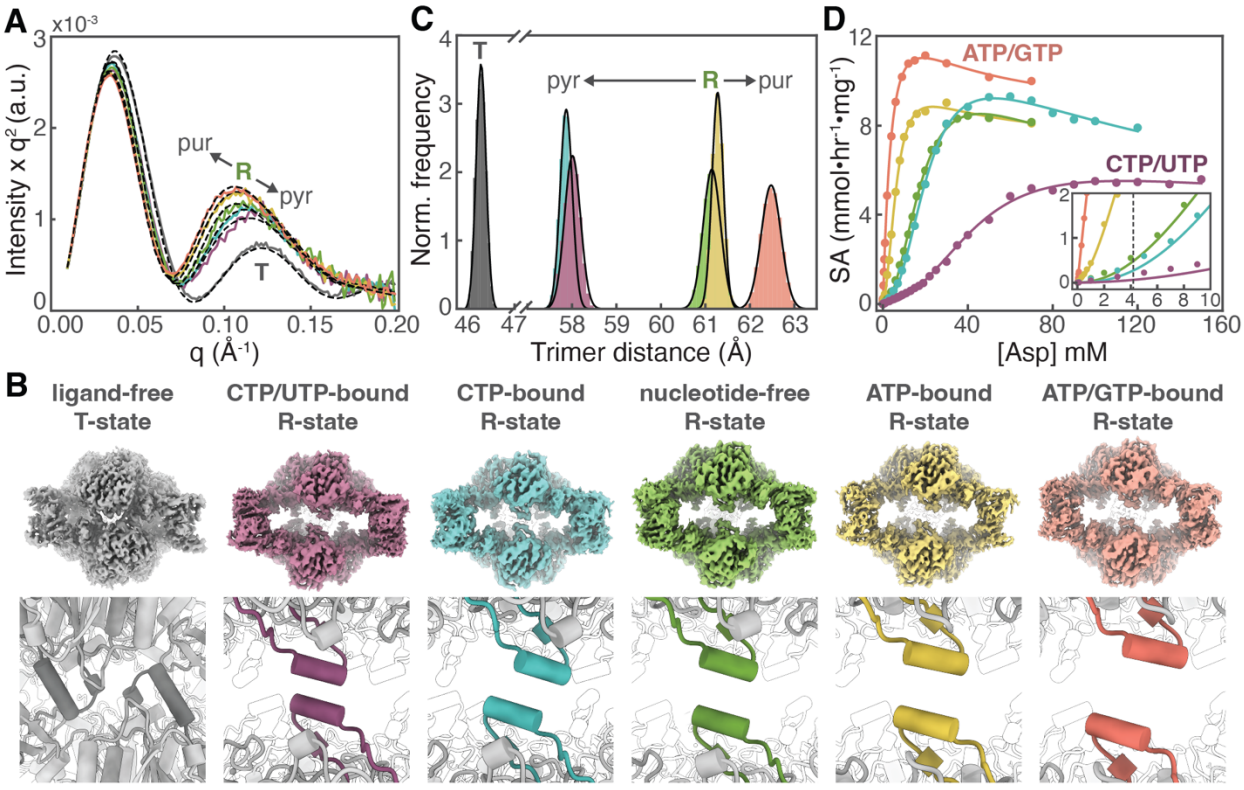

Figure 2. Effect of nucleotides on quaternary structure and activity of *E. coli* ATCase at pH 7.5 and 15 mM $MgCl_2$. No ligands were added to obtain the T-state. R-state conditions included substrate or substrate analogs and the following nucleotide compositions: 1.5 mM CTP, 1.5 mM UTP (*purple*), 1.5 mM CTP alone (*blue*), no nucleotides (*green*), 5 mM ATP (*yellow*), or 5 mM ATP, 1 mM GTP (*salmon*). **(A)** Scattering profiles obtained by SEC-SAXS reveal a gradient of R-states in addition to the ligand-free T-state (*solid curves*) and agree well with the theoretical scattering of cryo-EM models in panel B (*dashed curves*). The secondary peak positions indicate that purines and pyrimidines cause an expansion and compaction of the R-state, respectively. R-state conditions contained 500 μM CP, 10 mM succinate. **(B)** Cryo-EM under the same set of conditions as SEC-SAXS reveals a gradient of R-state structures in addition to a compact T-state. *Top:* Consensus maps of the ligand-free T-state (2.6 Å), CTP/UTP-bound R-state (3.1 Å), CTP-bound R-state (3.5 Å), R-state without nucleotides (3.1 Å), ATP-bound R-state (3.3 Å), and ATP/GTP-bound R-state (3.3 Å). *Bottom:* Refined consensus models show how nucleotides control the degree of separation between the 240s loops from the top and bottom catalytic trimers. **(C)** Structural heterogeneity within each of the states in panel B was characterized by 3D variability analysis and converted to particle distributions as a function of the center-of-mass distance between the trimers. The R-state ensembles produced by purines and pyrimidines do not overlap. **(D)** Specific activities of ATCase under the same set of nucleotide compositions as in panels A-C with 4.8 mM CP at variable Asp concentrations. CTP/UTP produces a highly sigmoidal curve, while ATP/GTP removes this effect. At high [Asp], the activities decrease due to behavior reminiscent of substrate inhibition.[31] *Inset:* Curves near physiological [Asp] of 4.2 mM.

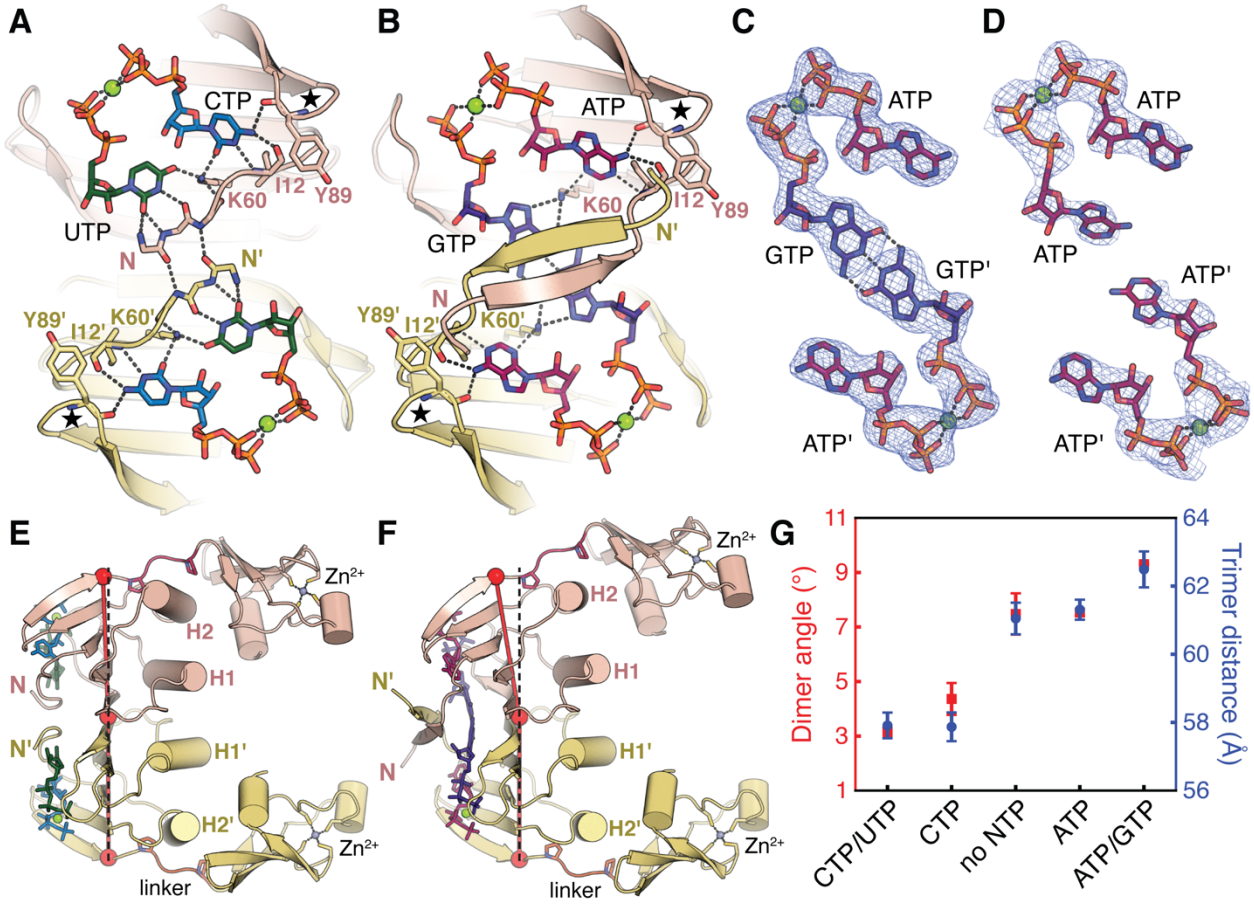

Figure 3: Structural basis of allosteric regulation by nucleotides. **(A)** Crystal structure of the CTP/UTP-bound R-state (PDB ID: 4kh1)[9] shows Y89 and I12 backbone interactions favor CTP in the first site, while N-terminal backbone interactions favor UTP in the second. K60 bridges the two sites, providing selectivity for both. **(B)** 2.2-Å crystal structure of ATP/GTP R-state obtained in this study at neutral pH. Like with CTP, ATP is favored in the first site, and K60 selects for GTP in the second. The GTPs form a non-canonical base pair at the dimer interface, stabilized by interactions with K60 and T43 on the interfacial β-strands (Supp. Fig. 20). N-termini form a domain-swapped β-sheet above the GTPs, creating a hydrophobic pocket. **(C)** Polder omit map of nucleotides in panel B, contoured at 6σ (*blue mesh*), support an ordered ATP in the first site and GTP in the second. **(D)** 3.0-Å crystal structure of ATP/ATP R-state obtained this study at near-neutral pH. Polder omit map contoured at 6σ (blue mesh) shows ATP is disordered in the second site. **(E)** Side view of regulatory dimer from cryo-EM CTP/UTP R-state model. Binding of CTP/UTP flattens the β-sheet across the dimer interface, placing the Zn-domains close together. One outer helix (H2) stays angled like in the T-state, while the other (H2′) straightens. **(F)** Side view of regulatory dimer from cryo-EM ATP/GTP R-state model. ATP/GTP produce the most bent β-sheet via domain-swapped N-terminal interactions, opening the Zn-domain distance. Both H2/H2′ helices straighten into a parallel arrangement. **(G)** Bending of the regulatory dimer controls the Zn-domain separation and correlates with the center-of-mass distance between the catalytic trimers. The dimer angle is defined by three points on the β-sheet (*red spheres*) and its deviation from planarity (*black dashed*) in panels E and F. In panels A and B, the outer loop (residues 88-89) is starred. In panels E and F, linker residues P97 and P100 are shown as sticks. Mg^{2+} ions are shown as green spheres.

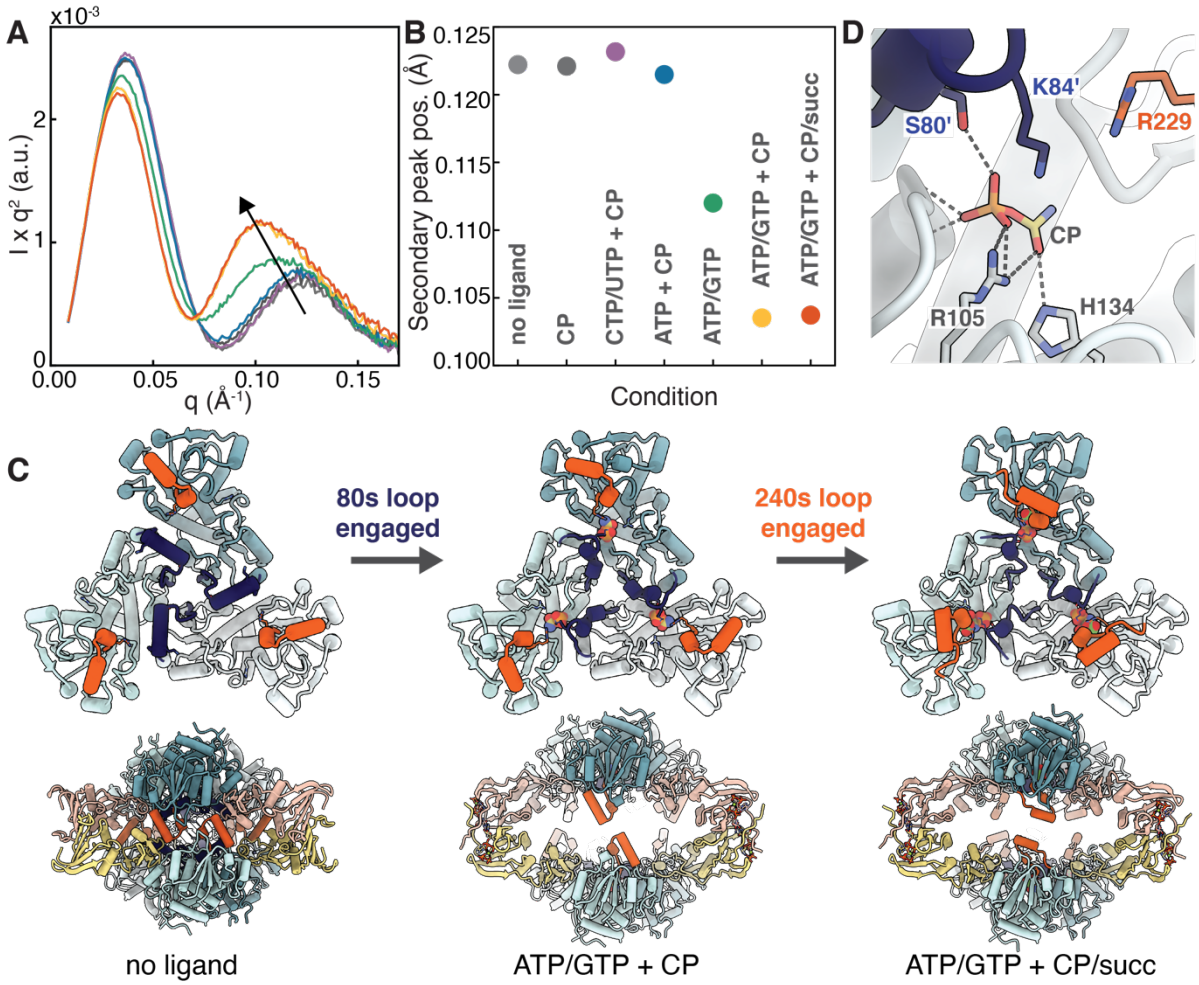

Figure 4. ATCase bypasses the T-state with the purine pair, ATP and GTP. **(A)** Scattering profiles of *E. coli* ATCase obtained by batch SAXS with and without 500 μM CP and **(B)** corresponding positions of secondary Kratky peak, shown with same color scheme. Consistent with our previous understanding of ATCase, CP alone (*dark gray*) is insufficient to cause a significant change from the ligand-free conformation (*light gray*), even with the addition of 1.5 mM CTP, 1.5 mM UTP (*purple*) or 5 mM ATP (*blue*). On the other hand, addition of 5 mM ATP, 1 mM GTP (*green*) is sufficient to cause a peak shift to lower *q* even in the absence of CP. When CP is included (*yellow orange*), the peak shifts all the way to the position of the ATP/GTP R-state (*red*). These results demonstrate the unique ability of the ATP/GTP pair to expand the quaternary structure, obviating the need for both substrates to bind to reach the R-state. **(C)** Cryo-EM model of ATCase obtained with 5 mM ATP, 1 mM GTP, 500 μM CP (*middle*) compared with those of the ligand-free T-state (*left*) and the ATP/GTP R-state (*right*) from Figure 2. A novel conformation is observed in which the 80s loops (*purple*) engaged but the 240s loops (*orange*) are not. **(D)** Close up of active site in novel conformation in panel C shows CP interacting the 80s loop (*purple*) from a neighboring subunit via S80 and K84. Engagement of the 240s loop (*orange*) with the second substrate involves interactions with both R229 and R234, but only R229 is near the active site when the loop is disengaged.

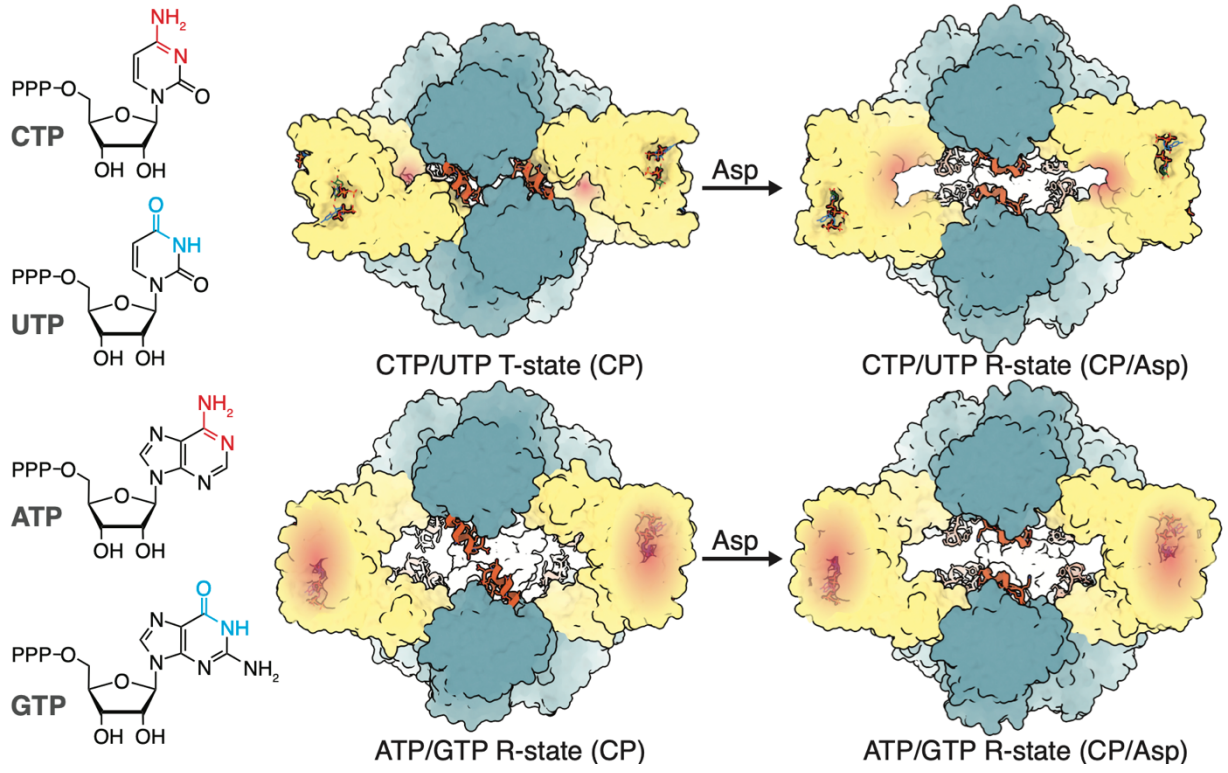

Figure 5. Model for nucleotide-dependent regulation of *E. coli* ATCase. The most physiological allosteric inhibitor is the CTP/UTP pair, while the most physiological allosteric activator is the ATP/GTP pair. Site 1 is specific for chemical features on the CTP and ATP nucleobases (*red*), while site 2 is specific for those on UTP and GTP (*cyan*). The enzyme's affinity for the second substrate, Asp, is determined by the ability of the 240s loop (*orange*) to move within the confined space of the enzyme cavity. *Top:* With CTP/UTP bound, the regulatory dimers (*yellow*) are pinched closed, holding the catalytic trimers (*blue*) close together. This imposes cooperativity among the active sites to transition from the T-state conformation to one in which the 240s loops are engaged with Asp. *Bottom:* With ATP/GTP bound, the regulatory dimers open, allowing the enzyme to bypass the T-state. In this expanded conformation, the enzyme behaves like dissociated catalytic trimers, removing cooperativity among active sites by allowing independent movement of the 240s loops.

Author contributions. R.C.M. and M.G.P. purified proteins and performed SAXS experiments. R.C.M. performed SAXS data analysis, kinetic modeling of assay data, cryo-EM experiments, and cryo-EM data processing, model building, and refinement. M.G.P. performed activity assays, kinetic modeling, and crystallographic and cryo-EM model building and refinement. M.G.P. and N.B. grew crystals and performed crystallography experiments. X.P. synthesized PALA. N.A. supervised the project, acquired funding, and performed data analysis. R.C.M., M.G.P., and N.A. made figures and wrote the manuscript.

Acknowledgements. The authors would like to thank Steve Meisburger, John Bacik, Darren Xu, Jason Kaelber, and the Phenix team for insightful discussions about SAXS, crystallography, and EM. We are grateful to Richard Gillilan and Qingqiu Huang for assistance at CHESS, Mariena Silvestry-Ramos and Katie Spoth and for assistance at CCMR, Frank Murphy at APS, Ivan Keresztes at the Cornell NMR facility, and the staff at NCCAT. We thank Cody Aplin, Michael Lynch, Raley Schweinfurth for experimental help as well as the Crane, Hyster, and Milner labs for sharing instruments. SAXS and room-temperature crystallography were conducted at the Center for High-Energy X-ray Sciences (CHEXS), which is supported by the National Science Foundation (BIO, ENG and MPS Directorates) under award DMR-2342336, and the Macromolecular Diffraction at CHESS (Mac-CHESS) facility, which is supported by award 1-P30-GM124166 from the National Institute of General Medical Sciences (NIGMS) and the National Institutes of Health (NIH). Cryo-crystallography was conducted at the Northeastern Collaborative Access Team beamlines, which are funded by the NIGMS from the NIH (P30 GM124165). This research used resources of the Advanced Photon Source, a U.S. Department of Energy (DOE) Office of Science User Fa-cility operated for the DOE Office of Science by Argonne National Laboratory under Contract No. DE-AC02-06CH11357. Cryo-EM data collection was performed at the Cornell Center for Materials Research (CCMR) as well as at the National Center for Cryo-EM Access and Training (NCCAT) in New York City, which is supported by the NIH Common Fund Transformative High Resolution Cryo-Electron Microscopy program grant number U24 GM129539. NMR and MS spectra acquisitions were performed at Cornell NMR and Chemistry Mass Spectrometry Facilities. N.A. would like to acknowledge Richard Honzatko for suggesting that we study this enzyme many years ago as well as prior discussions with Evan Kantrowitz and Patrice Vachette that inspired this study. R.C.M. received half-time support from CHEXS through a student appointment, and M.G.P. received support from the Cornell Provost Diversity Fellowship. This work was supported by NIH grant GM124847 and startup fund from Cornell University to N.A.

Data Availability Statement. Coordinates and structure factors for crystal structures have been deposited in the Protein Data Bank under the following accession codes: 9EEH and 9EEJ. Cryo-EM maps have been deposited to the Electron Microscopy Data Bank with accession codes: EMD-47956, EMD-47957, EMD-47958, EMD-47959, EMD-47960, EMD-47961, EMD-47963, EMD-47964, EMD-47965, EMD-47966. The associated atomic models have been deposited to the Protein Data Bank with accession codes: 9EEK, 9EEL, 9EEM, 9EEN, 9EEO, 9EEP, 9EEQ, 9EER, 9EES, 9EEU.

References

1. Gerhart, J. From feedback inhibition to allostery: the enduring example of aspartate transcarbamoylase. *FEBS J.* **281**, 612–620 (2014).
2. Pardee, A. B. & Yates, R. A. Pyrimidine biosynthesis in Escherichia coli. *J. Biol. Chem.* **221**, 743–756 (1956).
3. Pardee, A. B. & Yates, R. A. Control of pyrimidine biosynthesis in Escherichia coli by a feed-back mechanism. *J. Biol. Chem.* **221**, 757–770 (1956).
4. Gerhart, J. C. & Pardee, A. B. The enzymology of control by feedback inhibition. *J. Biol. Chem.* **237**, 891–896 (1962).
5. Wild, J. R., Loughrey-Chen, S. J. & Corder, T. S. In the presence of CTP, UTP becomes an allosteric inhibitor of aspartate transcarbamoylase. *Proc. Natl. Acad. Sci. U. S. A.* **86**, 46–50 (1989).
6. Honzatko, R. B., Lauritzen, A. M. & Lipscomb, W. N. Metal cation influence on activity and regulation of aspartate carbamoyltransferase. *Proc. Natl. Acad. Sci. U. S. A.* **78**, 898–902 (1981).
7. Mendes, K. R., Martinez, J. A. & Kantrowitz, E. R. Asymmetric allosteric signaling in aspartate transcarbamoylase. *ACS Chem. Biol.* **5**, 499–506 (2010).
8. London, R. E. & Schmidt, P. G. A model for nucleotide regulation of aspartate transcarbamylase. *Biochemistry* **11**, 3136–3142 (1972).
9. Cockrell, G. M. *et al.* New paradigm for allosteric regulation of Escherichia coli aspartate transcarbamoylase. *Biochemistry* **52**, 8036–8047 (2013).
10. Monod, J., Wyman, J. & Changeux, J. P. ON THE NATURE OF ALLOSTERIC TRANSITIONS: A PLAUSIBLE MODEL. *J. Mol. Biol.* **12**, 88–118 (1965).
11. Changeux, J.-P. & Rubin, M. M. Allosteric Interactions in Aspartate Transcarbamylase. III. Interpretation of Experimental Data in Terms of the Model of Monod, Wyman, and Changeux. *Biochemistry* **7**, 553–560 (1968).
12. Howlett, G. J., Blackburn, M. N., Compton, J. G. & Schachman, H. K. Allosteric regulation of aspartate transcarbamoylase. Analysis of the structural and functional behavior in terms of a two-state model. *Biochemistry* **16**, 5091–5100 (1977).
13. Hervé, G., Moody, M. F., Tauc, P., Vachette, P. & Jones, P. T. Quaternary structure changes in aspartate transcarbamylase studied by X-ray solution scattering. Signal transmission following effector binding. *J. Mol. Biol.* **185**, 189–199 (1985).
14. Kim, K. H., Pan, Z. X., Honzatko, R. B., Ke, H. M. & Lipscomb, W. N. Structural asymmetry in the CTP-liganded form of aspartate carbamoyltransferase from Escherichia coli. *J Mol Biol* **196**, 853–875 (1987).
15. Stevens, R. C. & Lipscomb, W. N. A molecular mechanism for pyrimidine and purine nucleotide control of aspartate transcarbamoylase. *Proc. Natl. Acad. Sci. U. S. A.* **89**, 5281–5285 (1992).
16. Xi, X. G. *et al.* The Activation of Escherichia coli Aspartate Transcarbamylase by ATP: Specific Involvement of Helix H2′ at the Hydrophobic Interface Between the Two Domains of the Regulatory Chains. *J. Mol. Biol.* **242**, 139–149 (1994).
17. Fetler, L. & Vachette, P. The allosteric activator Mg-ATP modifies the quaternary structure of the R-state of Escherichia coli aspartate transcarbamylase without altering the TR equilibrium. *J. Mol. Biol.* **309**, 817–832 (2001).
18. Wiley, D. C. *et al.* The 5.5 Angstrom resolution structure of the regulatory enzyme, asparate transcarbamylase. *Cold Spring Harb. Symp. Quant. Biol.* **36**, 285–290 (1972).
19. Ke, H. M., Lipscomb, W. N., Cho, Y. J. & Honzatko, R. B. Complex of N-phosphonacetyl-L-aspartate with aspartate carbamoyltransferase. X-ray refinement, analysis of conformational changes and catalytic and allosteric mechanisms. *J. Mol. Biol.* **204**, 725–747 (1988).
20. Jin, L., Stec, B., Lipscomb, W. N. & Kantrowitz, E. R. Insights into the mechanisms of catalysis and heterotropic regulation of Escherichia coli aspartate transcarbamoylase based upon a structure of the enzyme complexed with the bisubstrate analogue N-phosphonacetyl-L-aspartate at 2.1 A. *Proteins* **37**, 729–742 (1999).

21. Honzatko, R. B. *et al.* Crystal and molecular structures of native and CTP-liganded aspartate carbamoyltransferase from Escherichia coli. *J. Mol. Biol.* **160**, 219–263 (1982).
22. Stevens, R. C., Gouaux, J. E. & Lipscomb, W. N. Structural consequences of effector binding to the T state of aspartate carbamoyltransferase: crystal structures of the unligated and ATP- and CTP-complexed enzymes at 2.6-A resolution. *Biochemistry* **29**, 7691–7701 (1990).
23. Gouaux, J. E., Stevens, R. C. & Lipscomb, W. N. Crystal structures of aspartate carbamoyltransferase ligated with phosphonoacetamide, malonate, and CTP or ATP at 2.8-.ANG. resolution and neutral pH. *Biochemistry* **29**, 7702–7715 (1990).
24. Peterson, A. W., Cockrell, G. M. & Kantrowitz, E. R. A Second Allosteric Site in Escherichia coli Aspartate Transcarbamoylase. *Biochemistry* **51**, 4776–4778 (2012).
25. Cockrell, G. M. & Kantrowitz, E. R. Metal ion involvement in the allosteric mechanism of Escherichia coli aspartate transcarbamoylase. *Biochemistry* **51**, 7128–7137 (2012).
26. Moody, M. F., Vachette, P. & Foote, A. M. Changes in the x-ray solution scattering of aspartate transcarbamylase following the allosteric transition. *J. Mol. Biol.* **133**, 517–532 (1979).
27. Fetler, L., Tauc, P., Hervé, G., Moody, M. F. & Vachette, P. X-ray Scattering Titration of the Quaternary Structure Transition of Aspartate Transcarbamylase with a Bisubstrate Analogue: Influence of Nucleotide Effectors. *J. Mol. Biol.* **251**, 243–255 (1995).
28. Svergun, D. I., Barberato, C., Koch, M. H., Fetler, L. & Vachette, P. Large differences are observed between the crystal and solution quaternary structures of allosteric aspartate transcarbamylase in the R state. *Proteins* **27**, 110–117 (1997).
29. Collins, K. D. & Stark, G. R. Aspartate transcarbamylase. Interaction with the transition state analogue N-(phosphonacetyl)-L-aspartate. *J. Biol. Chem.* **246**, 6599–6605 (1971).
30. Bennett, B. D. *et al.* Absolute metabolite concentrations and implied enzyme active site occupancy in Escherichia coli. *Nat. Chem. Biol.* **5**, 593–599 (2009).
31. Pastra-Landis, S. C., Evans, D. R. & Lipscomb, W. N. The effect of pH on the cooperative behavior of aspartate transcarbamylase from Escherichia coli. *J. Biol. Chem.* **253**, 4624–4630 (1978).
32. Chen, H., Giese, T. J., Golden, B. L. & York, D. M. Divalent Metal Ion Activation of a Guanine General Base in the Hammerhead Ribozyme: Insights from Molecular Simulations. *Biochemistry* **56**, 2985–2994 (2017).
33. Sakash, J. B. & Kantrowitz, E. R. The N-terminus of the regulatory chain of Escherichia coli aspartate transcarbamoylase is important for both nucleotide binding and heterotropic effects. *Biochemistry* **37**, 281–288 (1998).
34. Dembowski, N. J. & Kantrowitz, E. R. The use of alanine scanning mutagenesis to determine the role of the N-terminus of the regulatory chain in the heterotropic mechanism of Escherichia coli aspartate transcarbamoylase. *Protein Eng. Des. Sel.* **7**, 673–679 (1994).
35. Kendrew, J. *et al.* A three-dimensional model of the myoglobin molecule obtained by X-ray analysis. *Nature* **181**, 662–666 (1958).
36. Muirhead, H. & Perutz, M. F. Structure Of Hæmoglobin: A Three-Dimensional Fourier Synthesis of Reduced Human Haemoglobin at 5.5 Å Resolution. *Nature* **199**, 633–638 (1963).
37. Meisburger, S. P., Xu, D. & Ando, N. REGALS: a general method to deconvolve X-ray scattering data from evolving mixtures. *IUCrJ* **8**, 225–237 (2021).
38. Bethell, M. R. & Jones, M. E. Molecular size and feedback-regulation characteristics of bacterial aspartate transcarbamulases. *Arch. Biochem. Biophys.* **134**, 352–365 (1969).
39. Kenny, M. J., McPhail, D. & Shepherdson, M. A reappraisal of the diversity and class distribution of aspartate transcarbamoylases in gram-negative bacteria. *Microbiology* **142 (Pt 7)**, 1873–1879 (1996).
40. Hofer, A., Crona, M., Logan, D. T. & Sjöberg, B. M. DNA building blocks: Keeping control of manufacture. *Critical Reviews in Biochemistry and Molecular Biology* vol. 47 50–63 Preprint at https://doi.org/10.3109/10409238.2011.630372 (2012).
41. Zimanyi, C. M. *et al.* Tangled up in knots: Structures of inactivated forms of E. coli class Ia ribonucleotide reductase. *Structure* **20**, 1374–1383 (2012).
42. Smith, J. L. *et al.* Structure of the allosteric regulatory enzyme of purine biosynthesis. *Science* **264**,

1427–1433 (1994).

43. Zhou, G., Smith, J. L. & Zalkin, H. Binding of purine nucleotides to two regulatory sites results in synergistic feedback inhibition of glutamine 5-phosphoribosylpyrophosphate amidotransferase. *J. Biol. Chem.* **269**, 6784–6789 (1994).
44. Chen, S. *et al.* Mechanism of the synergistic end-product regulation of Bacillus subtilis glutamine phosphoribosylpyrophosphate amidotransferase by nucleotides. *Biochemistry* **36**, 10718–10726 (1997).
45. Powers, S. G. & Meister, A. Mechanism of the reaction catalyzed by carbamyl phosphate synthetase. Binding of ATP to the two functionally different ATP sites. *J. Biol. Chem.* **253**, 800–803 (1978).
46. Jin, L., Stec, B., Lipscomb, W. N. & Kantrowitz, E. R. Insights into the mechanisms of catalysis and heterotropic regulation of Escherichia coli aspartate transcarbamoylase based upon a structure of the enzyme complexed with the bisubstrate analogue N-phosphonacetyl-L-aspartate at 2.1 A. *Proteins* **37**, 729–742 (1999).